Hindawi Publishing Corporation
International Journal of Antennas and Propagation
Volume 2015, Article ID 601835, 11 pages
http://dx.doi.org/10.1155/2015/601835

Research Article

Experimental Characterization and Correlation Analysis of Indoor Channels at 15 GHz

Xin Zhou,[1,2] Zhangdui Zhong,[1] Bei Zhang,[1] Ruisi He,[1] Ke Guan,[1] Qi Wang,[1] and David Matolak[3]

[1] *The State Key Laboratory of Rail Traffic Control and Safety, Beijing Jiaotong University, No. 3 Shang Yuan Cun, Haidian District, Beijing 100044, China*
[2] *National Institute of Metrology, No. 18 North Sanhuan Road, Chaoyang District, Beijing 100013, China*
[3] *Department of Electrical Engineering, University of South Carolina, 3A28 Swearingen Engineering Center, 301 South Main Street, Columbia, SC 29208, USA*

Correspondence should be addressed to Bei Zhang; zbandysun@gmail.com

Received 9 October 2014; Revised 11 February 2015; Accepted 12 February 2015

Academic Editor: Miguel Ferrando Bataller

The indoor radio channels at 15 GHz are investigated based on measurements. The large- and small-scale fading behaviors as well as the delay dispersion characteristics are discussed. It is found that the large-scale fading, Ricean K-factor, and delay spread can be described by log-normal distributions. Furthermore, both autocorrelation and cross correlation properties of the above parameters are analyzed and modeled. These parameters characterize fading and delay behaviors as well as their mutual dependency and can be used as empirical values for future wireless system design and simulation in 15 GHz short-range indoor channels.

1. Introduction

As the demand for cellular data has been growing at a staggering pace, with conservative estimates ranging from 40% to 70% per year [1], the requirement of larger network capacity as well as greater connectivity will be a huge problem in the future cellular communication system. According to the intermediate description of the spectrum needs and usage principles of Mobile and wireless communications Enablers for the Twenty-twenty Information Society (METIS), one of the spectrum challenges for next-generation (fifth-generation (5G)) mobile systems is to study new bands, in particular by extending the spectrum range for mobile communications to yet rarely used higher frequency bands (above 6 GHz) to support high data rate up to multigigabits per second [2, 3].

The 15 GHz band is another potential frequency spectrum resource for future network plans, and some 5G trails using the 15 GHz frequency band demonstrate data rates of 10 Gbps [4, 5]. The Radiocommunication Sector of the International Telecommunication Union (ITU-R) provides radio frequency channel arrangements for fixed wireless radio-relay systems operating in the 15 GHz (14.4–15.35 GHz) band [6]. The 15 GHz band is a portion in the microwave range of the 12–18 GHz electromagnetic spectrum, which is the so-called "Ku" band. Ku-band is primarily used for satellite communications, and there are also some mobile applications in this band; for example, see [7, 8]. The first- and second-order narrowband channel statistics, say the Doppler spread, delay spread, time share of connections, and time share of fades for the land mobile satellite channel in different outdoor environments at Ku-band, are presented in [9].

A better understanding of spatial and temporal characteristics at different frequency bands can be helpful in network planning, especially for the future large-scale multiantenna systems and networks. The spatial and temporal parameters such as Ricean K-factor, power delay profile (PDP) statistics, root mean square (RMS) delay spread, and angular spread at higher frequency bands in corridor environments have been studied for many years. For wideband indoor communication applications at higher frequency bands, the so-called millimeter wave (mmW) bands, between 30 and 300 GHz, are being actively studied in recent years [10–13]. A simple stochastic multipath channel model for the office environments acquired from a wideband channel sounder based on PN

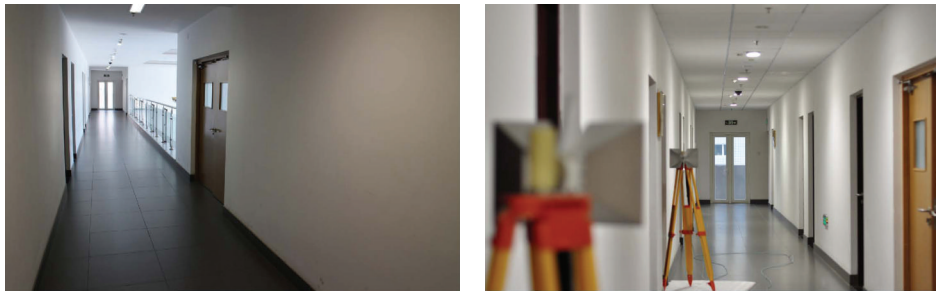

(a) Photograph of the measurement corridor A (b) Photograph of the measurement corridor B

Figure 1: Measurement environments, (a) corridor A, (b) corridor B.

sequences for the 60 GHz band is proposed in [14]. At the same spectrum, the statistical results such as RMS delay spread and corresponding tapped delay line (TDL) model are extracted by wideband impulse response measurements of an indoor radio channel [15]. The authors in [16] believe that 11 GHz is a challenging frequency for future mobile systems. The large-scale parameters such as path loss, shadowing, narrowband K-factor, delay spread, and coherence bandwidth are presented. As far as the authors know, there is little literature about the propagation characteristics and channel analysis at 15 GHz bands in indoor scenarios.

The description of the mutual dependency between the large-scale fading (LSF) and small-scale fading (SSF) as well as spatial and temporal characteristics of this wireless channel (cross correlation properties) is important for the implementation of realistic network level simulators for wideband mobile communication systems in indoor environments [17, 18]. The correlation properties for indoor propagation channel have been characterized based on wideband measurements [19–23]. The cross correlation of the LSF and SSF parameters of two separated subchannels, the autocorrelation of the LSF parameters of one single subchannel, and the correlation of the SSF parameters of the PDP for an ultrawideband system have been analyzed in [23]. The authors in [17] proposed that the spatial autocorrelation function of azimuth spread, delay spread, and shadow fading can all be modeled with an exponential decay function in typical urban, bad urban, and suburban environments. It has been widely verified that there exists a correlation between the time delay spread and angular spread in outdoor environments [17–19]. These conclusions are proposed based on test beds operating at 1.8 GHz, 1.9 GHz, and 5.2 GHz, respectively. As far as the authors know, the joint statistical properties of the fading parameters such as the LSF parameters, Ricean K-factor, and RMS delay spread in indoor environments at 15 GHz have not been well addressed in related literature. In this paper, we fill this gap.

The main contributions of this work are summarized as follows:

(1) estimations and analysis of the LSF parameters Ricean K-factor and RMS delay spread as well as their cumulative distribution functions (CDFs) and probability distribution functions (PDFs) based on indoor daytime experimental campaigns in the 15 GHz bands,

(2) empirical analysis of autocorrelation and cross correlation properties among the LSF, Ricean K-factor, and RMS delay spread.

This paper is organized as follows: the measurement campaign is described in Section 2. In Section 3, statistical channel parameters are introduced and extracted from measurement data. The spatial autocorrelation properties as well as cross correlation properties among LSF, Ricean K-factor, and RMS delay spread are analyzed in Section 4. A comparison of the joint statistical properties for other frequency bands in the same scenario with our results is presented in Section 5. Section 6 concludes the paper.

2. Measurement Campaign

2.1. Measurement Environment. Measurements are conducted along two corridors in the Mechanical Engineering Building on the campus of Beijing Jiaotong University, China, as shown in Figure 1. This is a 10-story building with classrooms and faculty offices. There is an open area on the north side of the building and a concrete building on the south side of the measurement region. The size of the corridor A is 1.90 m × 40.77 m and the ceiling height is 3 m. It has wooden doors with small windows to various rooms, and the walls are constructed from concrete materials, the floor ground is covered by glazed bricks, and the corridor ceiling is made of plastic materials. The transmitter (Tx) is fixed and denoted by the pentacle (see Figure 2). At the receiver side (Rx), the antenna is moved along a straight line at 25 different locations acting as a single-antenna user, which is denoted as a circle in Figure 2. In order to achieve spatial averaging, five spatially separated points are measured at each receiver location as suggested in [24]. One received point is at the center of one specific location facing the Tx directly, surrounded by the remaining four points as shown in Figure 3; these points are separated by approximately 2 wavelengths. Assuming that the phase of received signal is uniformly distributed, it is reasonable to average out the small-scale fading effect via these five positions. As a reference, the spatial sample separation in indoor channel is no greater than 2 m in the 450 MHz–6 GHz range depending on the time resolution of the measurement equipment and the type of multipath channels [25]. The small-scale sampling avoids large-scale averaging bias in the

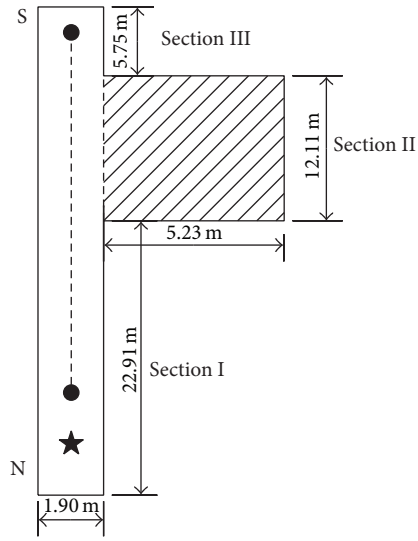

Figure 2: Layout of corridor A.

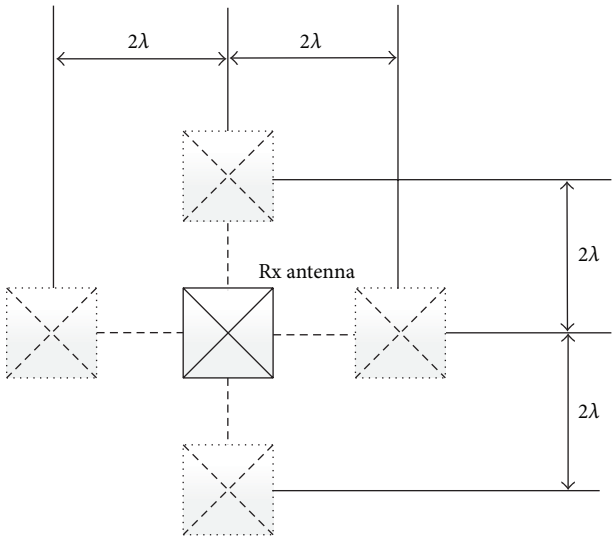

Figure 3: Positions of Rx at each location.

resulting small-scale statistics. Since there are no obstructions between the Tx and Rx, a dominant line-of-sight (LOS) component exists. It is worth mentioning that there is a 5.23 m × 12.11 m semi-open space along the corridor A, that is, the shadow region as depicted in Figure 2. As a result, the measurement environment can be divided into three regions due to the variation in these indoor propagation environments. The locations 1–10 fall into the corresponding region I, locations 11–21 lie in region II, and region III includes the rest. Finally, the measurements were conducted during the daytime with no people present in the area. Therefore the channel may be regarded as physically stationary or at least quasi stationary [15].

For the purpose of statistical analysis, we conducted another measurement in corridor B, which has the same size as corridor A; that is, the size of the corridor B is

Figure 4: Measurement system.

1.90 m × 40.77 m and the ceiling height is 3 m. The only difference between these two corridors is that there is no semi-open space in corridor B. Due to physical constraints, we select 17 different locations at Rx with the same separation distance. Consequently, there are 42 locations in total to study the large- and small-scale fading in this paper.

2.2. Measurement System. Our measurement system consists of an Anritsu Vector Network Analyzer (VNA) with Spectrum Analyzer MS2038C, high-gain directive antennas OBH08180, cables, connectors, and laptop. The Tx and Rx antennas are connected by long cables as shown in Figure 4. Calibrations are conducted to remove the attenuation and phase rotation of the connecting cables before every test. The output power of Tx is 0 dBm. The equivalent isotropic radiated power (EIRP) is 13.8 dB. And the range of acceptable input signal to VNA is −110 dBm~+30 dBm. The VNA equipment guarantees 85 dB dynamic range at the measured band, which ensures that all the significant multipath components can be measured and subsequently resolved. The single-input-single-output (SISO) frequency-domain measurements are performed over a 1 GHz bandwidth and centered at 15 GHz. The time resolution τ_{rms} is inversely proportional to the sweeping bandwidth BW_{mea}, namely,

$$\tau_{\text{res}} \approx \frac{1}{\text{BW}_{\text{mea}}}, \tag{1}$$

which yields 1 ns for a sweep bandwidth of 1 GHz. This should be sufficient to resolve all multipath components of indoor environments at the 15 GHz band. The intermediate frequency (IF) bandwidth of the VNA during the measurement campaign is 1 KHz. IF bandwidth can be reduced to lower the noise floor of the instrument. The data structure consists of the transmission scattering parameter $S_{21}(f)$ and phase information, divided into 1024 data points. With 1024 discrete frequency points to sample the channel, the frequency resolution nearly equals 1 MHz. The antennas used in measurements are directional horn antennas with a bandwidth of 1 GHz. The horn antennas, with 13.8 dBi of gain, have 58° and 42° elevation (E) and horizon (H) plane 10 dB beamwidth. The use of directive antenna (horn-to-horn) is common at higher frequency band (≥6 GHz) [12–15]. These high-gain directive horn antennas were adopted in order to overcome the considerable amount of path loss at 15 GHz

Table 1: Measurement parameters.

Parameter	Value
Center frequency	15 GHz
System bandwidth	1 GHz
IF bandwidth	1 KHz
EIRP	13.8 dB
Antenna polarization	Vertical
Antenna gain	13.8 dBi
Noise floor	−88 dBm
Time resolution	1 ns
Range	30 m

as well as to emulate sectored antenna systems proposed for potential indoor wireless communication applications in 5G. Moreover, high-gain horn antennas enable us to achieve adequate signal noise ratio (SNR) at the maximum distances (the worst case of SNR for corridors A and B is 19.8 dB); therefore, power amplifier is omitted. Both transmitted and received antennas are vertically polarized in the elevation plane and fixed on adjustable tripods about 1.4 m above the ground. The height of antenna is set to simulate the communication between two portable devices and it will not vary much for most personal applications. At each position, the channel is measured twice to reduce random error during each measurement as well as the effect of the thermal noise under the assumption of channel stationary. Therefore, 10 measurements of the snapshots have been taken at each location. Via spectrum analyzer measurements, we found no interference present in our corridor environments. As a result, we ignore it in our work. A summary of the measurement parameters is listed in Table 1.

3. Analysis of Measurements

3.1. Data Preprocessing. For a time-invariant wideband channel, the channel impulse response (CIR) can be expressed as

$$h(d,\tau) = \sum_{i=0}^{N-1} a_i(d)\, e^{-j\phi_i} \delta(\tau - \tau_i), \quad (2)$$

where a_i, ϕ_i, and τ_i denote the amplitude, phase, and delay of the ith multipath component, respectively, d denotes the distance between Tx and Rx, and N is the total number of multipath components. In the VNA system, the measured transmission scattering parameter $S_{21}(d, f)$ is the transfer function $H(d, f)$ of the radio channel. Therefore, we can get the empirical CIR by performing an inverse fast Fourier transform algorithm (IFFT) of the measured transmission scattering parameter $S_{21}(d, f)$, as

$$h(d,\tau) = \mathrm{IFFT}\left(S_{21}(d,f)\right). \quad (3)$$

The mean relative power at each bin of delay τ_i is specified by the PDP of the channel, defined as the square magnitude of the CIR:

$$P(d,\tau) = |h(d,\tau)|^2. \quad (4)$$

The PDP can be used to characterize the dispersion of a multipath channel in the delay domain, which is caused by the reflections and scattering in the environment. The PDP can be obtained directly via the VNA measurement data by IFFT; however, it should be further processed to achieve better accuracy. This amounts to removal of "likely noise" components. Therefore, those delay taps in the PDP (i.e., multipath components) with a power below the noise floor plus 6 dB were removed [26]. In order to ensure validity of the estimation for subsequent channel statistical parameters, the PDP should be averaged over a sliding window. It is necessary to have enough samples in the averaging window W so that sufficient accuracy of the estimation of the averaged PDP (APDP) can be achieved [27, 28]. Hence the average window W is 10, given that we measured the transmission scattering parameter $S_{21}(d, f)$ twice at each location (five points).

3.2. Estimation of the Statistical Channel Parameters

3.2.1. Coherence Bandwidth. As the separation of frequency within the channel transfer function increases, the fading behavior at one of the frequencies tends to be uncorrelated with respect to the other. This is due to the fact that the electrical path lengths of the multipath components will be significantly different. The correlation between the behaviors at these two frequencies will depend on the time spread caused by the environment (dispersion of path lengths and associated powers). The coherence bandwidth B_{coh} can therefore be derived via the frequency correlation function $R_H(\Delta f, d)$ [29], which is obtained in practice by the fast Fourier transform (FFT) of the APDPs, as follows:

$$R_H(\Delta f, d) = \int_{-\infty}^{\infty} \left(\left(\frac{\sum_{k=i}^{i+W-1} P(d, k\tau)}{W} \right) e^{-j2\pi\Delta f \tau} d\tau \right), \quad (5)$$

where Δf is the frequency difference and $P(d, k\tau)$ is the original PDP extracted from measurements with distinguishable multipath components. $R_H(\Delta f, d)$ is calculated for each of the five measured points at a given location, and then the PDPs are averaged in the window W to obtain a location-specific frequency correlation function. B_{coh} is defined as the smallest value of Δf when the frequency correlation coefficient drops below a certain threshold, say 0.5 [30] (with $R_H(0, d)$ normalized to unity). The frequency correlation function $R_H(\Delta f, d)$ is calculated at all measurement locations and we average it in time domian, yielding $R_H(\Delta f, d)$. An example plot of the estimated frequency correlation function at location 15 is depicted in Figure 5. The distance between Tx and Rx is 18 m.

It is found that over all the measurements, B_{coh} varies from 284.9 MHz to 356.2 MHz with a mean value of 305.2 MHz, which is much larger than the frequency resolution of our measurement system. In [31], the coherence bandwidth measured for 90% of receiver position at 0.5 correlation levels ranges from 327.2 MHz to 578.1 MHz at 60 GHz, which is larger than what we have found in the 15 GHz band. The estimated value of coherence bandwidth function for 0.5 correlation level in corridor environment using horn-to-horn antenna configuration, B_{coh}, is observed to have a mean of

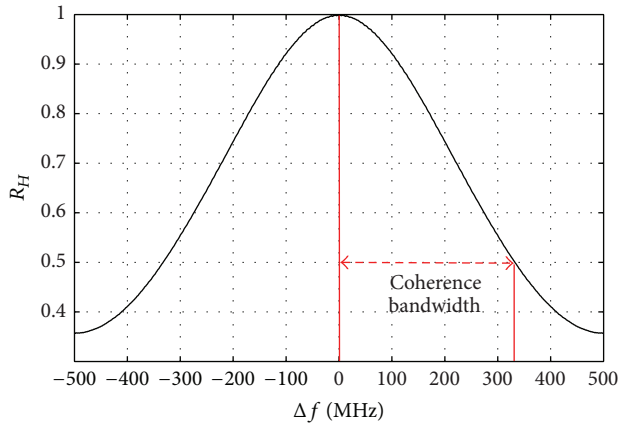

Figure 5: Example plot of frequency correlation function at location 15 of corridor A.

204.0 MHz at 62.4 GHz [32]. At that case, the Tx-Rx distance is 18.09 m.

3.2.2. Large-Scale Fading. In this paper, we use the classical log-distance linear function to fit the measured path loss. Thus, the averaged path loss in dB units can be represented as follows:

$$\overline{\mathrm{PL}}(d)\big|_{\mathrm{dB}} = \overline{\mathrm{PL}}(d_0) + 10\,n\log_{10}\left(\frac{d}{d_0}\right) + X_\sigma, \tag{6}$$

where n is the path loss exponent, $\mathrm{PL}(d_0)$ and d_0 denote the reference path loss and the reference distance, respectively. The averaged path loss at every location is computed using the mean value of the amplitude of the APDPs. For indoor scenarios, d_0 is typically fixed to 1 m [33, 34]. The large-scale fading component X_σ is typically modeled as a zero-mean Gaussian random variable. In our measurements, the power fluctuation is mainly introduced by deviation from the linear fit of received power over a large distance range and the amount of multipath available, although in any non-LOS conditions this variation is attributed to large objects shadowing the receiver [35]. As a consequence, we call this variation the large-scale fading (LSF).

3.2.3. Ricean K-Factor. A Rice distribution is used to describe the SSF characteristics in indoor environments with a strong LOS path for wideband systems [36, 37]. The Rice PDF is

$$f(r) = \frac{2(K+1)\,r}{\Omega} \times \exp\left(-K - \frac{(K+1)\,r^2}{\Omega}\right) I_0\left(2\sqrt{\frac{K(K+1)}{\Omega}}\,r\right), \tag{7}$$

where r is the small-scale fading amplitude which is calculated as the amplitude of the transfer function $H(d, f)$ after removal of the mean value and $I_0[\bullet]$ is the zero-order modified Bessel function of the first kind. At fixed location, the Ricean K-factor is the ratio of the power in the dominant LOS component to that in the noncoherent "scattered" components within the multipath profile, which can be a good indicator of the fading depths. The Ricean K-factor can be estimated by a moment-based method proposed in [38–40], which is given by

$$K = \frac{\sqrt{1 - \mathrm{Var}\left[P(d)\right] / \left(E\left[P(d)\right]\right)^2}}{1 - \sqrt{1 - \mathrm{Var}\left[P(d)\right] / \left(E\left[P(d)\right]\right)^2}}, \tag{8}$$

where $E[\bullet]$, $\mathrm{Var}[\bullet]$ denote the expected value and variance of $[\bullet]$, respectively. The estimation of K factor is also extracted from the data after application of the sliding window W mentioned before to observe the variation of the Ricean K-factor against distance.

3.2.4. Delay Spread. In order to characterize the delay dispersion of a multipath channel, the mean excess delay τ and RMS delay spread σ_τ are calculated. The mean excess delay is the first moment of the power delay profile and is defined by [25]

$$\overline{\tau} = \frac{\sum_{k=1}^{N} P(\tau_k)\,\tau_k}{\sum_{k=1}^{N} P(\tau_k)}. \tag{9}$$

The RMS delay spread is the second moment of the PDP and takes into account the relative powers of the taps as well as their delays, making it a good indicator of system performance in the presence of time dispersion. It is defined by [41]

$$\tau_{\mathrm{RMS}} = \sqrt{\frac{\sum_{i=1}^{N} P(\tau_i)\,\tau_i^2}{\sum_{i=1}^{N} P(\tau_i)} - \overline{\tau}^2}. \tag{10}$$

RMS delay spread is a good indicator of the system error rate performance for moderate delay spreads (within one symbol duration). If it is much less than the symbol duration, no significant ISI is encountered and the channel may be approximated as nondispersive. Thus, RMS delay spread serves as a convenient way of comparing different wideband channels [41].

3.3. Statistical Results. In total, 430,080 wideband PDPs are recorded in 42 locations during the measurement campaign. A snapshot frequency response and PDP obtained from measurements in corridor A after normalization to the calibrated signal at location 15 are shown in Figure 6. It shows the variation of channel frequency response measured at frequencies between 14.5 GHz and 15.5 GHz at location 15, and the Tx-Rx separation is 18 m. A strong LOS component (around 10 ns) can be observed in Figure 6. The quasi periodicity seen in the magnitude response in Figure 6(a) suggests a possible strong reflection in addition to the LOS plus weaker multipath components (i.e., a quasi-two-ray effect). Figure 7 shows the estimated results of Ricean K-factor versus distance factor in corridor A and corridor B. It is noted that the total variation of Ricean K-factor is not significant, and generally it decreases with the Tx-Rx separation. Ricean K-factor of every location in corridor B is larger than the ones in corridor A. It can be explained by the wave guide effect

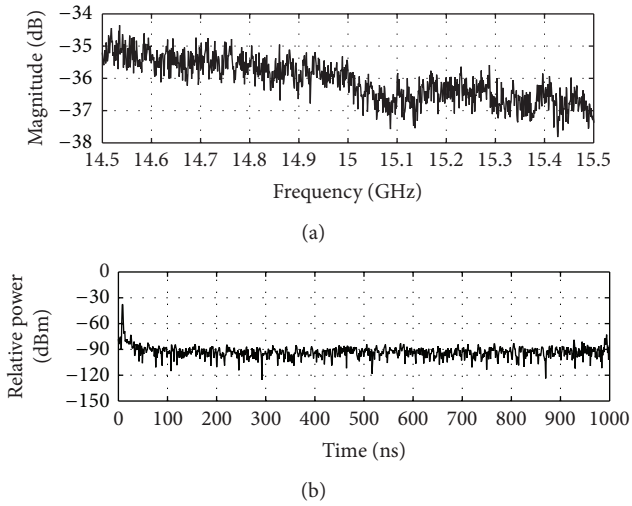

FIGURE 6: Snapshot received signal magnitude versus frequency domain (a) and time domain (b) of location 15 in corridor A.

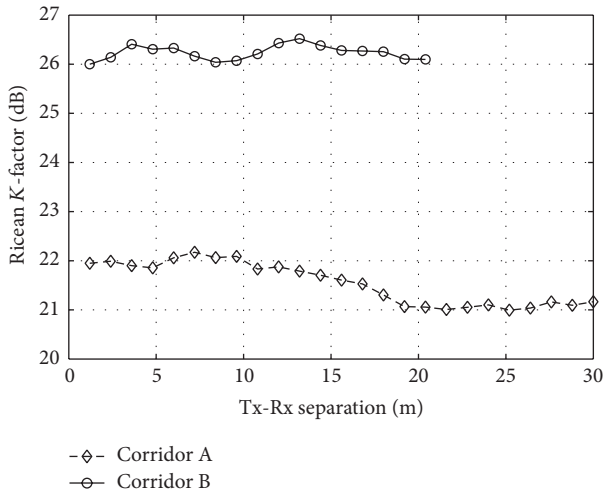

FIGURE 7: Ricean K-factor versus link distance.

since there is no semi-open space in corridor B and the LOS path contributes more to the received power. Next, the measurement results from delay dispersion parameters are summarized as follows (see Figure 8).

(i) Mean excess delay: over the range of measurement, the mean excess delay τ was found to have a median value of 67.4 ns and 39.5 ns, a maximum value of 191.8 ns and 82.4 ns, and 48.2 ns and 23.2 ns standard deviation for corridor A and corridor B, respectively. It increases linearly with the distance between Tx and Rx, which is similar to the conclusion in [42].

(ii) RMS delay spread: the static RMS delay is found to have a median value of 75.4 ns and 37.5 ns, a maximum value of 259.3 ns and 120.7 ns, and 71.1 ns and 27.2 ns standard deviation for corridor A and corridor B, respectively. The results versus link distance are illustrated in Figure 8. It is found that the RMS

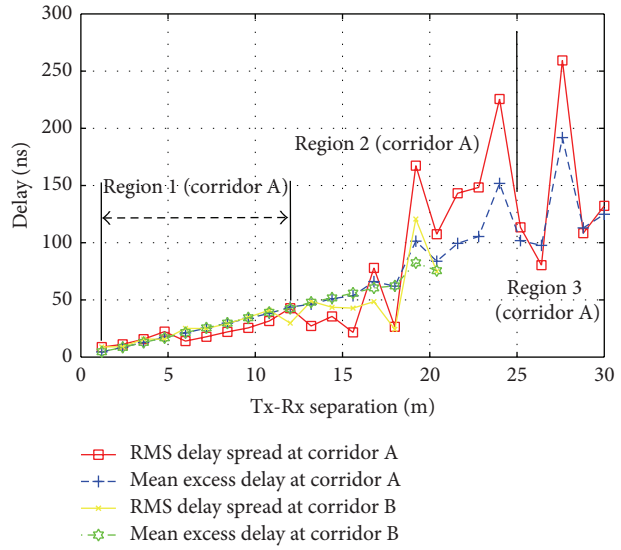

FIGURE 8: RMS delay spread versus link distance.

delay spread approximately increases with the Tx-Rx distance. We also note that the open area leads to a significant increase of the measured RMS delay spread in corridor A.

In order to investigate the statistical distribution of these channel parameters, we use the nonparametric test, that is, Kolmogorov-Smirnov (KS) test with a certain CI to compare the channel parameter sample with a reference probability distribution. The statistic of KS test is defined as the maximum value of the absolute difference between the CDF of the channel parameter X and the CDF of the estimated distribution E, which can be expressed as [43]

$$D_{\mathrm{KS}} = \sup_x \left| F_X(x) - F_E(x) \right|, \tag{11}$$

where $\sup_x$ is the supremum of the set of distances and $F(\bullet)$ denotes the CDF of $(\bullet)$. To test the goodness of fit, D_{KS} is compared to a threshold D_{th} corresponding to a given significance level α. Set $\alpha = 5\%$ in our analysis; then the CI of KS test is 95%. Any fitting distribution for which $D_{\mathrm{KS}} \geq D_{\mathrm{th}}$ is rejected with significance 95%; otherwise, it is accepted with the same level of significance. Table 2 summarizes the KS passing rate of the zero-mean Gaussian fitting distribution for LSF, Ricean-K factor, and RMS delay spread in our corridor measurement environments. It is found that a log-normal distribution accurately fits the statistical distributions of LSF, Ricean K-factor, and RMS delay spread, which is similar to the results in [17]. The statistical distributions of the LSF (X_σ), Ricean K-factor, and RMS delay spread over the entire set of measurements are shown in Figures 9–11. Figures 10 and 11 suggest that the Ricean K-factor and RMS delay spread can also be described by Gaussian distribution function, but the goodness of fit is inferior to that for LSF. All the statistical distribution parameters of them are listed in Table 3.

Table 2: KS test passing rate of the Gaussian distribution.

Parameter	KS passing rate (%)	Critical value (%)
Large-scale fading	91.87	20.52
Ricean K-factor	99.23	20.52
RMS delay spread	77.31	20.52

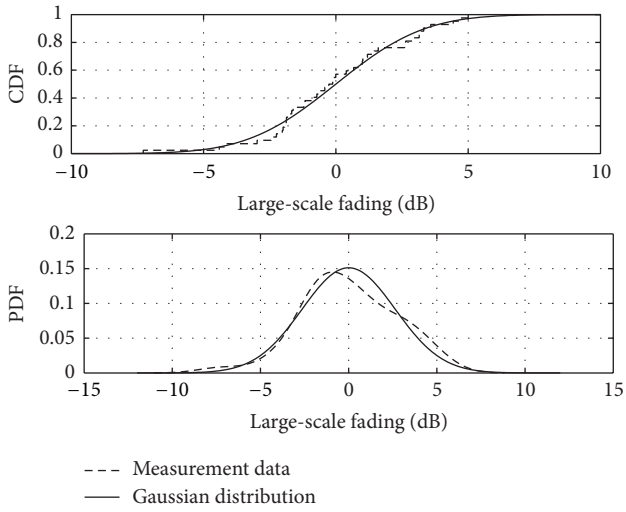

Figure 9: CDF and PDF of the measured large-scale fading, together with a Gaussian fit.

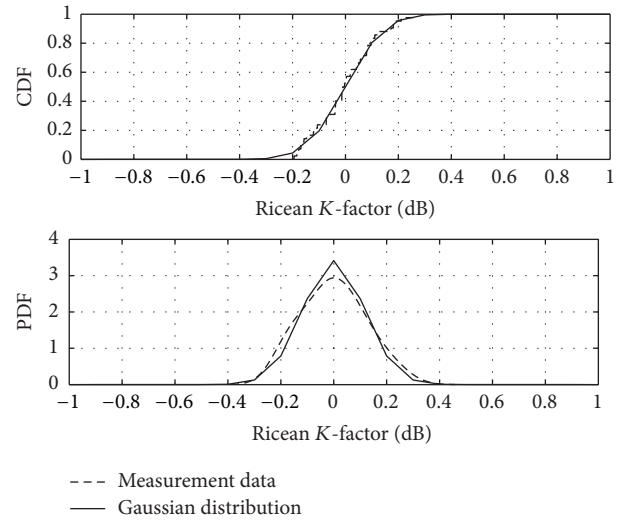

Figure 10: CDF and PDF of the measured Ricean K-factor, together with a Gaussian fit.

4. Correlation Properties

In this section, the spatial autocorrelations as well as the cross correlations among different statistical channel parameters are investigated based on measurements. For simulating a wireless channel, the joint random behaviors among LSF, Ricean K-factor, and RMS delay spread are required, as stated in [17–19]. The authors in [12, 41] show that small-scale fading parameters (such as Ricean K-factor) are correlated

Table 3: Distribution parameters.

Statistical parameters		Value
Large-scale fading [dB]	σ_{LSF}	2.01
RMS delay spread [ns]	μ_{RMS}	60.1
	σ_{RMS}	59.99
Ricean K-factor [dB]	μ_K	23.4
	σ_K	0.43

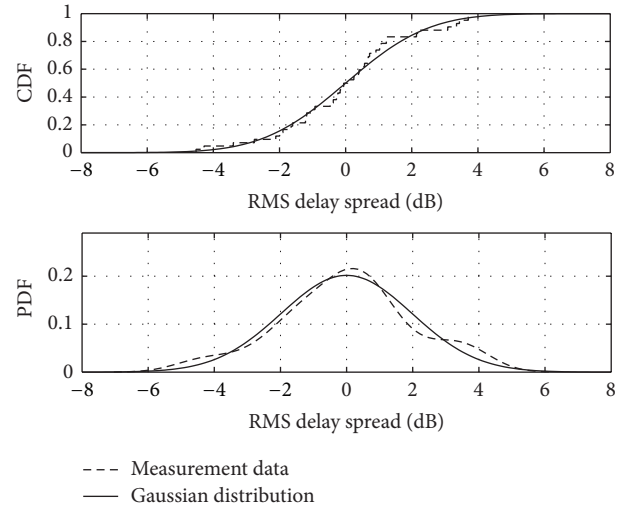

Figure 11: CDF and PDF of the RMS delay spread, together with a Gaussian fit.

with the RMS delay spread. However, there is no empirical investigation on the cross correlation properties of channel parameters in an indoor scenario at 15 GHz. In order to investigate the cross correlation properties of RMS delay spread and Ricean K-factor, the distance dependency of $10\log_{10}(\tau_{\text{rms}})$ and $10\log_{10}(K)$ should be firstly removed by using a Least-Square (LS) fit, as

$$\tau_{\text{RMS-LS}} = 10\log_{10}(\tau_{\text{RMS}}) - \langle 10\log_{10}(\tau_{\text{RMS}})\rangle,$$
$$K_{\text{LS}} = 10\log_{10}(K) - \langle 10\log_{10}(K)\rangle, \quad (12)$$

where $\langle\bullet\rangle$ operator generates the distance-dependent LS regression model of term $(\bullet)$. The deviations are found to be normally distributed in dB units.

The spatial autocorrelation functions of these parameters are shown in Figures 12–14. The correlation distance is defined where the spatial autocorrelation decreases to e^{-1}. It indicates that the correlation distance of LSF, RMS delay spread, and Ricean K-factor are about 3.2, 4.6, and 7 m, respectively. We found that a single exponential decaying function accurately models the spatial autocorrelation function of the LSF; the spatial autocorrelation function of the Ricean K-factor can be fitted with a zero-order of first kind Bessel function; and a double exponential decaying function accurately models the spatial autocorrelation function of RMS delay spread. The tunable parameters of fitting functions

Table 4: Spatial autocorrelation fitting parameters.

Fitting variables	Model type	Goodness of fit		
		SSE	R-square	RMSE
LSF	$A1 * \exp(-B1 * x) + (1 - A1)$	0.107	0.953	0.095
Ricean K-factor	$A2 * \text{besselj}(0, B2 * x) + (1 - A2)$	0.061	0.989	0.056
RMS delay spread	$A3 * \exp(B3 * x) + (1 - A3) * \exp(C3 * x)$	0.199	0.929	0.105

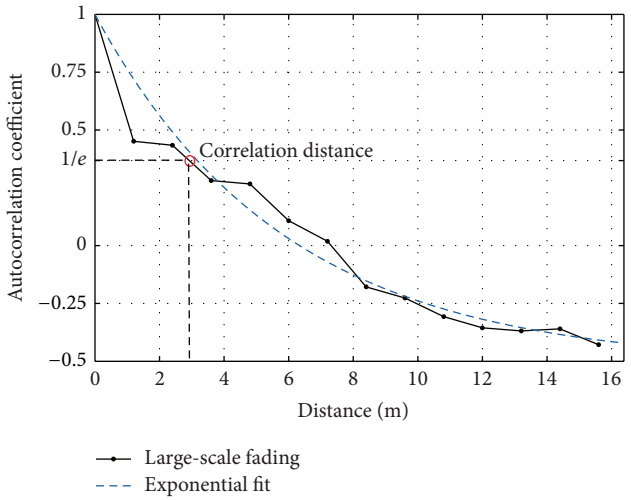

Figure 12: Empirical spatial autocorrelation function of large-scale fading with an exponential fit.

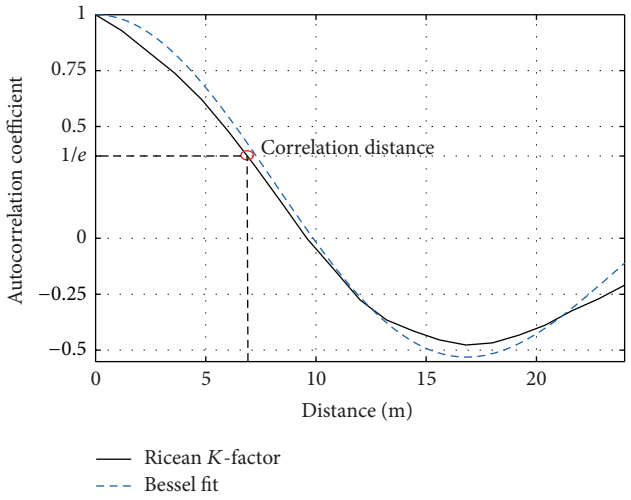

Figure 13: Empirical spatial autocorrelation function of Ricean K-factor with a zero-order first kind Bessel fit.

are obtained by using the LS fit method with 95% confidence bounds. Fitting parameters are summarized in Table 4.

The cross correlation coefficient, ρ, is defined as the Pearson product moment correlation coefficient:

$$\rho = \frac{n\sum x_i y_i - \sum x_i \sum y_i}{\sqrt{n\sum x_i^2 - \left(\sum x_i\right)^2}\sqrt{n\sum y_i^2 - \left(\sum y_i\right)^2}}, \quad (13)$$

Table 5: Cross correlation coefficients.

Parameters	Coefficient
LSF versus RMS delay spread	0.20
Ricean K-factor versus RMS delay spread	−0.35
LSF versus Ricean K-factor	−0.59

Table 6: Correlation distance in [45–47].

	Correlation distance [m]		
Delay spread	7	8	7
Shadow fading	6	10	10
Ricean K-factor	6	4	15

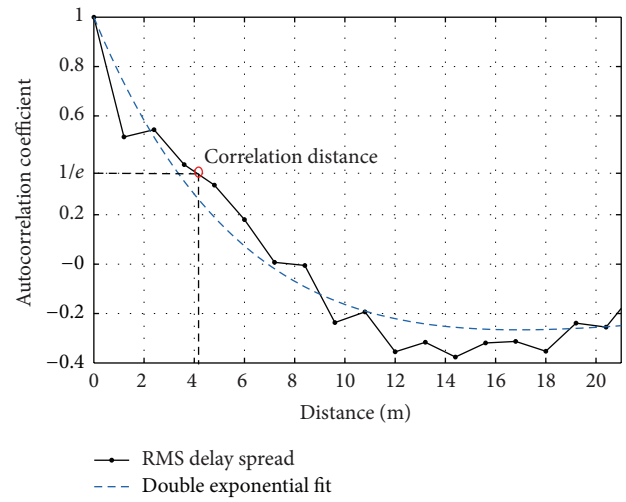

Figure 14: Empirical spatial autocorrelation function of RMS delay spread with a double exponential fit.

where x, y represent any two parameters of the set {LSF, Ricean K-factor, and RMS delay spread} (without distance dependency) and n is the number of samples, that is, the number of locations ($n = 42$). Cross correlation coefficients of these parameters can be found in Table 5. Note that there is a positive cross correlation between the LSF and RMS delay spread. The RMS delay spread $\tau_{\text{RMS-LS}}$ and Ricean K-factor K_{LS} are observed suggesting that the mechanisms leading to delay dispersion and SSF are also related, although they are not as strongly anticorrelated as the correlation between LSF

Table 7: Cross correlation coefficients in another frequency band.

Scenario	Corridor (LOS, 1.9 GHz)	Indoor office (LOS, 2–6 GHz)	InH (LOS, 2–6 GHz)	3D-UMi (LOS, 2–6 GHz)
Delay spread versus SF	0.88	−0.6	−0.8	−0.4
Delay spread versus Ricean K-factor	−0.85	−0.6	−0.5	−0.7
SF versus Ricean K-factor	−0.93	0.4	0.5	0.5

and SSF. This matches the theoretical predictions reported in [44], where a proportional function is used to model RMS delay spread with Ricean K-factor. It can also be inferred that the LSF X_σ and Ricean K-factor K_{LS} are negatively correlated, indicating that the mechanisms leading to LSF and SSF of channel are related.

5. Discussion

In this section, some comparisons and heuristic explanations for the measured results are provided.

5.1. Results in Open Literature. For comparison, the correlation parameters in [18] and some standard channel models [45–47] are summarized in Tables 6 and 7. It can be concluded that the correlation distances of our 15 GHz indoor measurement tend to be smaller than the results in Table 6 since the size of the spatial stationary region in indoor scenarios is smaller than outdoors; the Ricean K-factor may exhibit variations even over small regions, which can be another reason for the variation of Ricean K-factor as mentioned in previous section. The cross correlation coefficients in Table 7 tend to be larger than those in our measurement.

5.2. Correlation Analysis. The cross correlation properties among the LSF, RMS delay spread, and Ricean K-factor can be explained as follows. Large LSF values are usually associated with an increase of scatterers, which will lead to more multipath components; therefore, the Ricean K-factor decreases with the increase of LSF. What is more, it is a reasonable assumption that the shortest delay components have the most power. The distribution of PDPs may be more uniformed with a deeper fading and thus leads to a higher delay spread.

The wave guiding effect may also cause a different behavior of cross correlation properties among statistical parameters between the indoor channel and outdoor channel (and between our indoor corridor and a more "open" office environment of the WINNER case). For corridor measurements, wave guiding effects of the radio wave propagation occur along the corridor at larger values of link distance. At small distances, the reflected wave components are rejected by the directional receiver antenna and the wave guiding effect is not dominant. However, for the large distance region, reflected wave components are close to the LOS path and are received by the receiver antenna. The total received signal is stronger than it should be from free space propagation and the transmitted wave propagates in a guided fashion [20]. Moreover, with the increase of frequency band, contribution of reflected components reduces, and the channel characteristic is getting significantly changed [25]. Therefore, the cross correlation properties among the shadow fading, Ricean K-factor, and RMS delay spread will be different compared with the correlation results in [18, 45–47].

From a system design viewpoint, these empirical correlation trends also suggest that the potential space and frequency diversity gains are relatively correlated, since a low delay spread results in a high coherence bandwidth (hence a low frequency diversity gain) while low values of delay spread also mean large spatial correlations (hence a low spatial diversity gain).

6. Summary

In this paper, measurement-based correlation analysis of the 15 GHz indoor wideband channel has been presented. Statistical wideband channel parameters including the LSF standard deviation, Ricean K-factor, and delay dispersion were estimated and modeled using log-normal variables. The spatial autocorrelation functions of LSF, Ricean K-factor, and RMS delay spread can be described by a single exponential function, a zero-order of Bessel function of first kind, and a double exponential function, respectively. Measurements show that there is stronger negative cross correlation between the Ricean K-factor and LSF than that between the Ricean K-factor and RMS delay spread. Moreover, the RMS delay spread is slightly positively correlated with LSF. The results are useful for 15 GHz indoor channel simulation and system design.

Conflict of Interests

The authors declare that there is no conflict of interests regarding the publication of this paper.

Acknowledgments

This work is supported by State Laboratory of Rail Traffic Control and Safety Project (nos. RCS2011ZZ002 and RCS2014ZT32) of Beijing Jiaotong University, the National 863 Project under Grant no. 2014AA01A706, the National Natural Science Foundation of China under Grant no. U1334202, the Fundamental Research Funds for the Central Universities (Grants nos. 2014JBZ021and 2014RC018), and the Key Grant Project of Chinese Ministry of Education no. 313006.

References

[1] UMTS Forum, *Mobile Traffic Forecasts: 2010–2020 Report*, vol. 44, UMTS Forum, 2011.

[2] A. Apostolidis, L. Campoy, K. Chatzikokolakis et al., "Intermediate description of the spectrum needs and usage principles," METIS Deliverable D5.1, 2013.

[3] Y. Wang, J. Li, L. Huang, Y. Jing, A. Georgakopoulos, and P. Demestichas, "5G mobile: spectrum broadening to higher-frequency bands to support high data rates," *IEEE Vehicular Technology Magazine*, vol. 9, no. 3, pp. 39–46, 2014.

[4] Ericsson, "NTT DOCOMO to trial 5G with Ericsson," 2014, http://www.ericsson.com/news/1783524.

[5] J. Stewart, "5G will require new as well as established spectrum bands, but the availability of new bands is not confirmed," Analysys Mason, 2014, http://www.analysysmason.com/About-Us/News/Newsletter/5G-spectrum-Oct2014/.

[6] ITU-R Rep. F. 636-4, "Radio frequency channel arrangements for fixed wireless systems operating in the 14.4-15.35 GHz Band," 2012.

[7] J. Dutronc and J. N. Colcy, "Land mobile communications in Ku-band. Results of a test campaign on EUTELSAT I-F1," *International Journal of Satellite Communications*, vol. 8, no. 1, pp. 43–63, 1990.

[8] G. Butt, B. G. Evans, and M. Richharia, "Narrowband channel statistics from multiband propagation measurements applicable to high elevation angle land-mobile satellite systems," *IEEE Journal on Selected Areas in Communications*, vol. 10, no. 8, pp. 1219–1226, 1992.

[9] S. Scalise, H. Ernst, and G. Harles, "Measurement and modeling of the land mobile satellite channel at Ku-band," *IEEE Transactions on Vehicular Technology*, vol. 57, no. 2, pp. 693–703, 2008.

[10] R. C. Daniels, J. N. Murdock, T. S. Rappaport, and R. W. Heath Jr., "60 GHz wireless: up close and personal," *IEEE Microwave Magazine*, vol. 11, no. 7, pp. S44–S50, 2010.

[11] T. S. Rappaport, S. Sun, R. Mayzus et al., "Millimeter wave mobile communications for 5G cellular: it will work!," *IEEE Access*, vol. 1, pp. 335–349, 2013.

[12] S. Nie, G. R. MacCartney Jr., S. Sun, and T. S. Rappaport, "72 GHz millimeter wave indoor measurements for wireless and backhaul communications," in *Proceedings of the IEEE 24th Annual International Symposium on Personal, Indoor, and Mobile Radio Communications (PIMRC '13)*, pp. 2429–2433, September 2013.

[13] M. Jacob and T. Kürner, "Radio channel characteristics for broadband WLAN/WPAN applications between 67 and 110 GHz," in *Proceedings of the 3rd European Conference on Antennas and Propagation (EuCAP '09)*, pp. 2663–2667, March 2009.

[14] T. Zwick, T. J. Beukema, and H. Nam, "Wideband channel sounder with measurements and model for the 60 GHz indoor radio channel," *IEEE Transactions on Vehicular Technology*, vol. 54, no. 4, pp. 1266–1277, 2005.

[15] N. Moraitis and P. Constantinou, "Measurements and characterization of wideband indoor radio channel at 60 GHz," *IEEE Transactions on Wireless Communications*, vol. 5, no. 4, pp. 880–889, 2006.

[16] M. Kim, Y. Konishi, Y. Chang, and J. I. Takada, "Large scale parameters and double-directional characterization of indoor wideband radio multipath channels at 11 GHz," *IEEE Transactions on Antennas and Propagation*, vol. 62, no. 1, pp. 430–441, 2014.

[17] A. Algans, K. I. Pedersen, and P. E. Mogensen, "Experimental analysis of the joint statistical properties of azimuth spread, delay spread, and shadow fading," *IEEE Journal on Selected Areas in Communications*, vol. 20, no. 3, pp. 523–531, 2002.

[18] C. Oestges, D. Vanhoenacker-Janvier, and B. Clerckx, "Channel characterization of indoor wireless personal area networks," *IEEE Transactions on Antennas and Propagation*, vol. 54, no. 11, pp. 3143–3150, 2006.

[19] C.-C. Chong, C.-M. Tan, D. I. Laurenson, S. McLaughlin, M. A. Beach, and A. R. Nix, "A new statistical wideband spatio-temporal channel model for 5-GHz band WLAN systems," *IEEE Journal on Selected Areas in Communications*, vol. 21, no. 2, pp. 139–150, 2003.

[20] H. Xu, V. Kukshya, and T. S. Rappaport, "Spatial and temporal characteristics of 60-GHZ indoor channels," *IEEE Journal on Selected Areas in Communications*, vol. 20, no. 3, pp. 620–630, 2002.

[21] C.-C. Chong, D. I. Laurenson, and S. McLaughlin, "Spatio-temporal correlation properties for the 5.2-GHz indoor propagation environments," *IEEE Antennas and Wireless Propagation Letters*, vol. 2, no. 1, pp. 114–117, 2003.

[22] D. L. Ndzi, N. Savage, and B. Gremont, "Spatial and temporal variation of wideband indoor channels," *International Journal of Antennas and Propagation*, vol. 2010, Article ID 735434, 11 pages, 2010.

[23] R. Zhang, Y. Zhang, Z. Zhong, and X. Lu, "The correlation properties of subchannel fading for non-continuous carrier aggregation based on indoor ultra-wideband measurement," in *Proceedings of the IEEE Global Communications Conference (GLOBECOM '12)*, pp. 3931–3935, December 2012.

[24] R. Sun and D. W. Matolak, "Characterization of the 5-GHz elevator shaft channel," *IEEE Transactions on Wireless Communications*, vol. 12, no. 10, pp. 5138–5145, 2013.

[25] T. S. Rappaport, *Wireless Communications Principles and Practice*, Prentice Hall, 2nd edition, 2001.

[26] A. F. Molisch and M. Steinbauer, "Condensed parameters for characterizing wideband mobile radio channels," *International Journal of Wireless Information Networks*, vol. 6, no. 3, pp. 133–154, 1999.

[27] W. C. Y. Lee, "Estimate of local average power of a mobile radio signal," *IEEE Transactions on Vehicular Technology*, vol. 34, no. 1, pp. 22–27, 1985.

[28] E. Bonek, M. Herdin, W. Weichselberger, and H. Ozcelik, "MIMO—study propagation first!," in *Proceedings of the 3rd IEEE International Symposium on Signal Processing and Information Technology (ISSPIT '03)*, pp. 150–153, 2003.

[29] A. F. Molisch, *Wireless Communications*, John Wiley & Sons, 2nd edition, 2010.

[30] G. L. Stüber, *Principles of Mobile Communication*, Springer, 2011.

[31] A. Hammoudeh, D. A. Scammell, and M. G. Sánchez, "Measurements and analysis of the indoor wideband millimeter wave wireless radio channel and frequency diversity characterization," *IEEE Transactions on Antennas and Propagation*, vol. 51, no. 10, pp. 2974–2986, 2003.

[32] M. O. Al-Nuaimi and A. G. Siamarou, "Coherence bandwidth characterisation and estimation for indoor Rician multipath wireless channels using measurements at 62.4 Ghz," *IEE Proceedings: Microwaves, Antennas and Propagation*, vol. 149, no. 3, pp. 181–187, 2002.

[33] J. D. Parsons, *The Mobile Radio Propagation Channel*, Wiley, London, UK, 2nd edition, 2000.

[34] ITU-R Reports, "Propagation data and prediction models for the planning of indoor radio communication systems and local area networks in the frequency range 900 MHz to 100 GHz," Tech. Rep. P. 1238-4, ITU-R Reports, 2005.

[35] B. M. Donlan, D. R. McKinstry, and R. M. Buehrer, "The UWB indoor channel: large and small scale modeling," *IEEE Transactions on Wireless Communications*, vol. 5, no. 10, pp. 2863–2872, 2006.

[36] U. G. Schuster and H. Bölcskei, "Ultrawideband channel modeling on the basis of information-theoretic criteria," *IEEE Transactions on Wireless Communications*, vol. 6, no. 7, pp. 2464–2474, 2007.

[37] V. Hovinen, M. Hämäläinen, and T. Pätsi, "Ultra wideband indoor radio channel models: preliminary results," in *Proceedings of the IEEE Conference on Ultra Wideband Systems and Technologies (UWBST '02)*, pp. 75–80, IEEE, Baltimore, Md, USA, May 2002.

[38] L. J. Greenstein, D. G. Michelson, and V. Erceg, "Moment-method estimation of the Ricean K-factor," *IEEE Communications Letters*, vol. 3, no. 6, pp. 175–176, 1999.

[39] A. Abdi, C. Tepedelenlioglu, M. Kaveh, and G. Giannakis, "On the estimation of the K parameter for the rice fading distribution," *IEEE Communications Letters*, vol. 5, no. 3, pp. 92–94, 2001.

[40] R. He, Z. Zhong, B. Ai, J. Ding, Y. Yang, and A. F. Molisch, "Short-term fading behavior in high-speed railway cutting scenario: Measurements, analysis, and statistical models," *IEEE Transactions on Antennas and Propagation*, vol. 61, no. 4, pp. 2209–2222, 2013.

[41] S. Saunders and A. Aragón-Zavala, *Antennas and Propagation for Wireless Communication Systems*, John Wiley & Sons, 2nd edition, 2007.

[42] R. J. C. Bultitude, P. Melancon, H. Zaghloul, G. Morrison, and M. Prokki, "The dependence of indoor radio channel multipath characteristics on transmit/receive ranges," *IEEE Journal on Selected Areas in Communications*, vol. 11, no. 7, pp. 20–30, 1993.

[43] F. J. Massey, "The Kolmogorov-Smirnov test for goodness of fit," *Journal of the American Statistical Association*, vol. 46, no. 253, pp. 68–78, 1951.

[44] K. Witrisal, Y.-H. Kim, and R. Prasad, "A new method to measure parameters of frequency-selective radio channels using power measurements," *IEEE Transactions on Communications*, vol. 49, no. 10, pp. 1788–1800, 2001.

[45] P. Kyosti, J. Meinila, L. Hentila et al., *WINNER II Channel Models*, WINNER II Public Diliverable IST-WINNER D1.1.2 version 1.1, 2007.

[46] ITU, "Guidelines for evaluation of radio interface technologies for IMT-advanced," ITU-R Rep. M. 2135, ITU Publications, 2009.

[47] 3rd Generation Partnership Project (3GPP), "Study on 3D channel model for LTE," Tech. Rep. TR36.873, 2014.